6.1 Introduction

Our environment is greatly affected by technological evolution since it contaminates the air, water, and earth through various human activities like industrial wastage, agricultural practices, mining, oil spilling etc. which eventually threatens human health and the destruction of the world's ecosystem [1]. Release of substances such as toxic gases, heavy metal ions, organic compounds, etc. have been on the rise as a result of an increase in the manufacturing of dyes, medications, pesticides, cosmetics, and leather [2]. In pharmaceutical and chemical industries, certain isomers of dihydroxybenzene, such as catechol (CT) and hydroquinone (HQ), have been extensively employed as raw materials for cosmetics, dyes, and insecticides. Due to their high levels of pollution, the European Union and the United States Environmental Protection Agency (EUUSEPA) have listed them in the category of dangerous environmental pollutants [3]. As a result, there is a high demand for a cost-effective, trustworthy, and quick technique of catechol and hydroquinone detection. These situations necessitate the careful contamination monitoring in order to prevent a terrible outcome. Chromatography, fluorescence, spectrometry, and chemiluminescence are some of the methods that are frequently used to detect CT and HQ, although most of them have limitations due to the expenditure involved in running the equipment, real-time analysis, and pre-treatment of samples [4]–[6]. Therefore, scientists have focused on electrochemical approaches to create a novel sensor that has high sensitivity, rapid detection, ease of use, and continuous monitoring of environmental pollutants. Due to its straightforward operational setup, high sensitivity, and strong selectivity, the electrochemical approach can be a promising alternative to solve such shortcomings [7]. In an electrochemical sensor the analyte undergoes redox reactions which is indicated by a signal in the form of current, electrical potential or some other electrical signals [8]. Due to the structural and chemical similarities between CT and HQ, when utilising common electrodes like glassy carbon, carbon paste, gold electrode, etc., the oxidation and reduction peaks of both isomers overlap. In order to detect CT and HQ simultaneously, customised electrodes containing various electrocatalytic materials such as conductive polymers, nanomaterials, and carbon materials have been designed [9] .

The interesting properties of metal organic frameworks (MOF), a novel class of hybrid material, include large surface area and programmable nanopores. Due to its very porous nature, it provides a perfect environment for guest accommodation in its unique nanochannels, offering versatility as regards special motion, charge transfer, magnetic, electronic, phase change, and other features [10]. Over the years, an immense number of MOFs are being developed, opening up new possibilities for gas separation, absorption, and sequestration [11]. The MOF's application to the catalytic process is driven by the redox active sites found in it. The MOF's application to catalytic activities is driven by the presence of redox active sites [12]. The instability of pure MOF thin layer in aquatic environments and its poor electrical conductivity provide difficulties when used to change the electrode surface. Introduction of conducting materials with excellent conductivity and electrocatalytic property can intensify the transfer of electron between redox active sites and electrodes and augment the electrochemical reactions rate by decreasing the overpotential of electrochemical sensor reactions [13]. Nonetheless, recent work on the combination of MOF-derived carbon and an appropriate conductive matrix has yielded good sensitivity and selectivity for CT and HQ. Chen et al. created composites of ZIF-8C MOF and graphene oxide by carbonising ZIF and decreasing GO for CT and HQ detection [14]. They used the electrode to analyse real water samples and discovered that it has great sensitivity and good performance. They also achieved a low LOD value with high dependability. Another group developed an electrochemical sensing unit for DBI detection using magnetic Ni@graphene composites with a core-shell structure (C-SNi@G) obtained from thermal annealing of Ni-BTC MOF [15]. Their CV tests revealed that the modified electrode produces two distinct oxidation peaks of HQ and CT. The MOF composites containing graphene oxide have also shown good electrocatalytic activity and high selectivity towards HQ and CT, with reported LODs ranging from 0.33 to 0.59 M. Abdel-Aziz et al. proposed an electrochemical sensor for catechol sensing based on a multi-walled carbon nanotube-poly(1,5-diaminonaphthalene) composite coated glassy carbon electrode (MWCNTs/p-DAN/GCE). They obtained a linear response with a LOD value of 1.01 M (S/N = 3) over a range of 2.01 to 1.31 M [16] . Manjunatha et al. reported an improved graphene paste electrode (PAMGPE) containing Poly (Adenine) for separating HQ and CT using Resorcinol (RC). The oxidation was observed to rise linearly in CT concentration peak current in the range of 2-8 μM and 1x 10^{-5}-1.5 x 10^{-4} M with a detection

limit of 2.4x 10^{-7} M [17]. In this chapter, PEDOT-inserted UiO-66 was employed as a working electrode for electrochemical sensing of HQ and CT individually as well as simultaneously. As already discussed in chapter 4, the PEDOT@UiO-66 MOF system has demonstrated an enhanced electrical conductivity as compared to its host UiO-66 counterpart. Therefore, the material was fabricated in ITO glass for the investigation of its redox activities through various methods like CV, EIS, and scan-rate dependent CV in a 3-electrode system using a potentiostat. The results of those experiments are discussed in the following sections. In the later sections, the qualitative and quantitative analysis of the sensing behaviour of PEDOT@UiO-66 for the analytes HQ and CT is discussed. The stability, reproducibility, and selectivity aspects of the electrode were also included here. Lastly, the analyte detection in a real sample has been highlighted in the chapter.

6.2 Electrochemical properties of PEDOT@UiO-66 coated working electrode

6.2.1 Cyclic voltammetry

To evaluate the electrochemical performance of PEDOT@UiO-66, the Cyclic Voltammetry (CV) and Electrochemical Impedance Spectroscopy (EIS) studies were performed with 5.0 mM [Fe $(CN)_6]^{3-/4-}$ containing 0.1M PBS of pH 7.2 as electrolyte. In Fig. 6.1 (a), we compared the CV of ITO, UiO-66 and PEDOT@UiO-66 in a voltage sweep of -0.2 V to 0.8 V, where the area under the curve represents the charge stored due to faradic and non-faradic processes. Redox peaks at 0.34 and 0.2 represent oxidation of Fe^{2+} species to Fe^{3+} and reduction of Fe^{3+} species to Fe^{2+}. From the voltammograms redox peak separation ΔE has been calculated for bare ITO, UiO-66 coated ITO and PEDOT@UiO-66 coated ITO as tabulated in Table 6.1 (a). It is found that upon coated with UiO-66 and PEDOT@UiO-66, the ΔE of ITO decreases to ~ 115 mV. The UiO-66 provides the adsorption sites for the electrons taking part in reaction with [Fe $(CN)_6]^{3-/4-}$ which is evident from the declined value peak -to-peak separation ΔE = $E_{pc} - E_{pa}$ indicating about the enhancement in number of electrons taking part in the reaction [19]. The cathodic peak current (I_{pc}) and anodic peak current (I_{pa}) are highest in PEDOT@UiO-66 amongst all the electrodes (374 μA and -375 μA). This is due the conducting nature of PEDOT which has been incorporated in the framework of UiO-66. The voltammograms of PEDOT@UiO-66

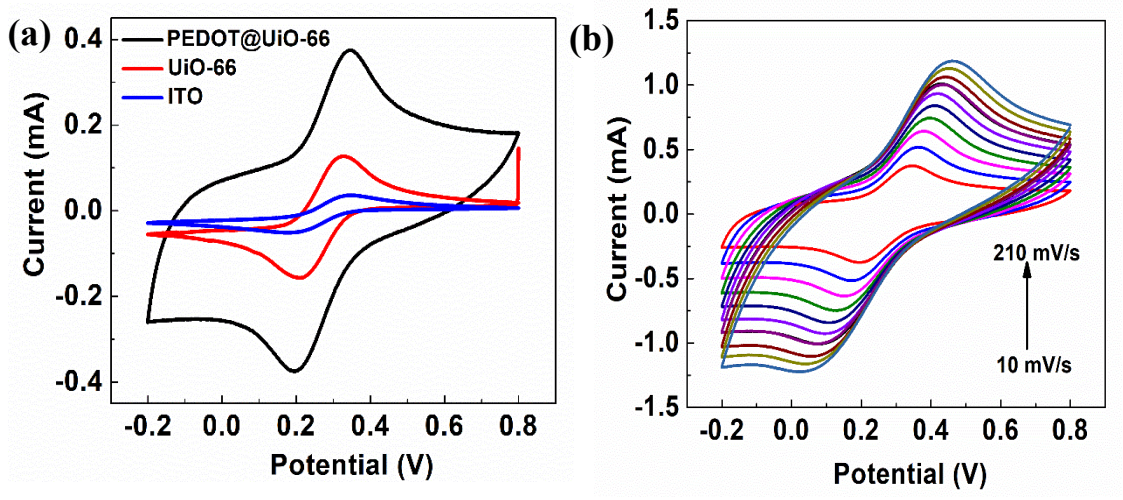

Fig. 6.1. (a) CV of ITO UiO-66 and PEDOT@UiO-66 (b) scan rate varying CV of PEDOT@UiO-66.

Table 6.1 Summary of CV results of ITO, UiO-66, PEDOT@UiO-66 systems

Electrode	Peak Separation ΔE (V)	Peak Current (oxidation) I_{pc} (mA)	Peak Current (Reduction) I_{pa} (mA)
ITO	0.211	0.035	-0.05
UiO-66	0.1141	0.127	-0.154
PEDOT@UIO-66	0.1215	0.374	-0.374

The charges due to various processes can be found out by using the relation –

$$I_p = av^b \qquad (6.1)$$

with different sweep rates showed a strong linear dependency in the range of 10 mV/s to 210 mV/s (Fig. 6.1 (b)). where a and b are adjustable parameters and b can be calculated from the slope of log-log plot of peak current (I_p) and scan rate (v). The value b suggests the process of charge storage undergoing in the electrode while scanning [18]. Since in our case the slopes of both cathodic and anodic processes are ~ 0.45 (Fig. 6.2 (a)), it says that the charge transfer was governed by adequate diffusion-controlled process. This means, the peak current will be proportional to the square root of scan rate which fits with Randles-Sevcik equation -

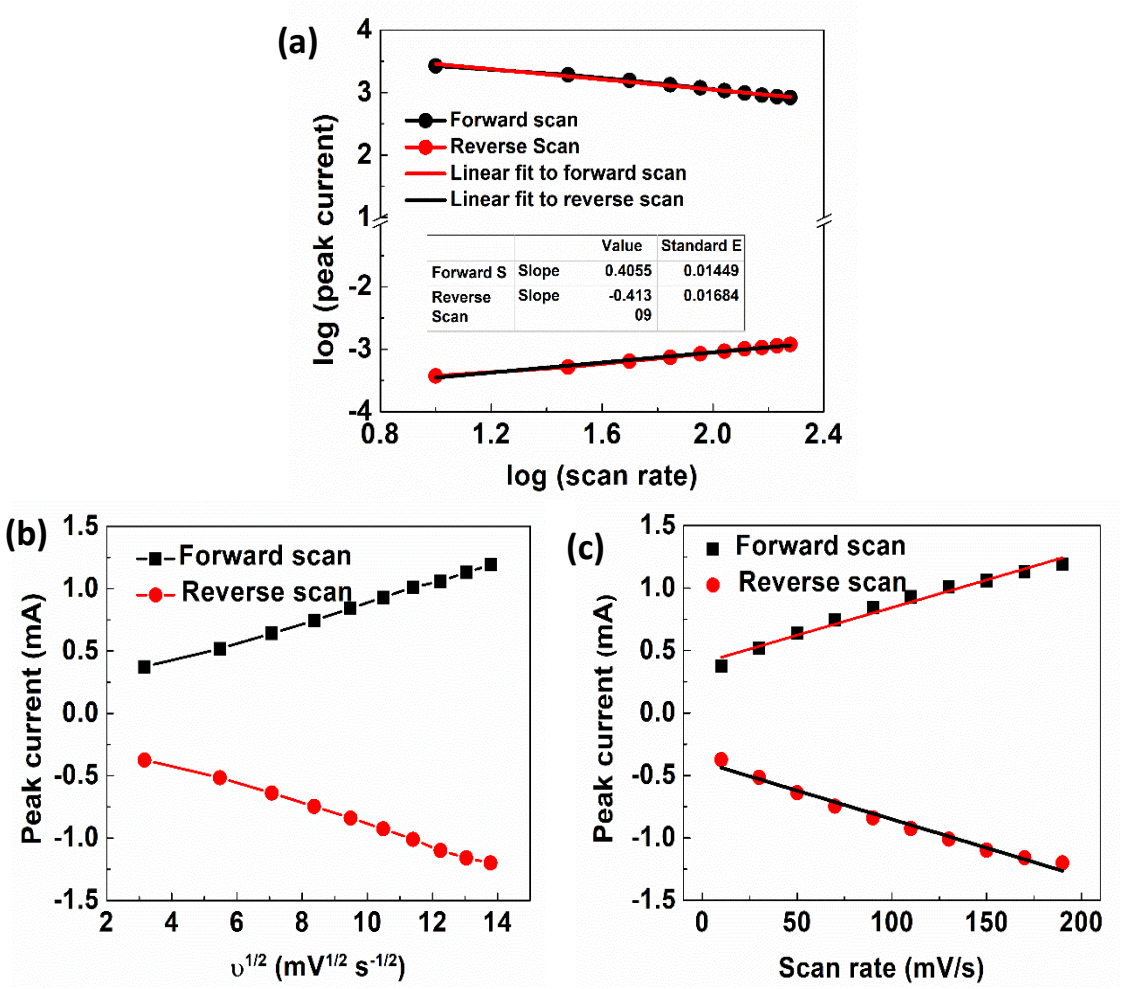

Fig. 6.2. (a) log-log peak current vs. scan rate (b) peak current vs. square root of scan rate (c) peak current vs. scan rate of PEDOT@UiO-66.

$$I_p = 0.446nFAC^o\left(\frac{nFvD_o}{RT}\right)^{1/2} \quad (6.2)$$

Electroactive surface area (A) can be calculated using eqn. (6.2) where D_o is the diffusion constant of analytes, C^o is the concentration of the analyte, F is Faraday's constant, n is the number of electrons taking part in the reaction [19].

The linear regression equation is given by

$$I_{pa} = 7.869\times v^{1/2} + 1.001\times 10^{-4}, R^2 = 0.9974 \quad (6.3)$$

$$I_{pc} = -8.123\times v^{1/2} + (-8.32\times 10^{-5}), R^2 = 0.9952 \quad (6.4)$$

As can be found in Fig. 6.2 (b), the plot for I_p vs. $\upsilon^{1/2}$ shows a good linear dependency with regression coefficients 0.9974 and 0.9952. The calculated electroactive area using the slop of I_p vs. $\upsilon^{1/2}$ and eqn. (5.2) is 1.89 cm^2. To be mentioned, the redox active sites are believed to be covered in this area of prepared electrode. The surface concentration of redox active sites is proportional to the slope of i_p vs. υ plot. By fitting this plot into Brown-Anson equation concentration of the same can be calculated [20]-

$$i_p = \frac{n^2 F^2 C_i A \upsilon}{4RT} \tag{6.5}$$

A good linear response was observed during the scan-rate varying CV which got fitted to eqn. (6.5). Using the slope of scan-rate vs. peak current we have calculated surface concentration of active sites, i.e., 4.70 x 10^{-9} mol/cm^2 (Fig. 6.2 (c)).

6.2.2 Electrochemical impedance spectroscopy

When an AC potential is applied to the electrochemical system the Faradic and non-Faradic processes take place at the electrode-electrolyte interface that encounters a complex resistance. Impedance spectroscopy unprevails the components of this frequency dependent complex impedance of the electrochemical system. The semicircle for ITO is largest among all the plots with R_{ct}= 914.9 Ω as depicted in Fig. 6.3(a). Moreover, PEDOT@UiO-66 has the lowest semicircle with R_{ct} of 121.16 Ω indicating the easy charge transfer process between the components. In the equivalent circuit (Fig. 6.3 (b)), R_s is the solution resistance and CPE is the constant phase element arises due to the non-ideal double layer capacitance formed at the electrode electrolyte interface. The linear part of the Nyquist plot at the lower frequency side of real axis is due to the diffusion of components present in the electrolyte known to be Warburg impedance(W). An additional CPE is present in the circuit which could be due to space charge layers between PEDOT and UiO-66 grains. When PEDOT is incorporated into the framework it enhances charge transfer the between electrode and electrolyte as it would carry delocalised charges along its backbone. This was revealed by the lower value of R_{ct} in PEDOT@UiO-66 in comparison to UiO-66 host.

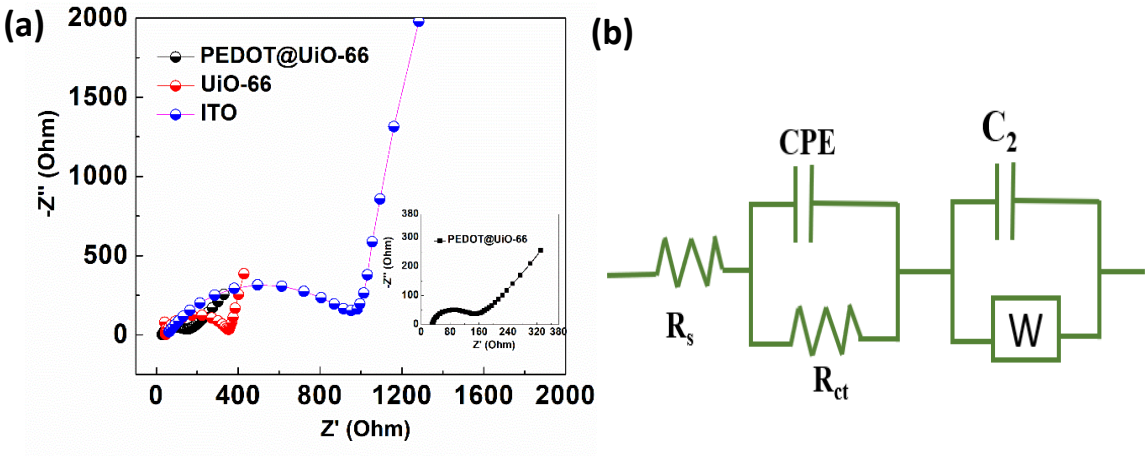

Fig. 6.3. (a) EIS of ITO, UiO-66, PEDOT@UiO-66 (b) equivalent circuit used to fit the Nyquist plot.

Table 6.2 Parameters obtained from the EIS equivalent circuit for different electrodes.

Electrode	**R_s (Ω)**	**R_{ct} (Ω)**	**C_2 (F)**	***W* x10^{-3} (S.$s^{1/2}$)**	***a* x10^{-3}**	**Y_o, x10^{-6} (S.s^a)**
ITO	55.36	914.9	9.13 x10^{-6}	0.428	744.2	0.45
UiO-66	46.02	311.7	3.186 x10^{-3}	0.913	865.3	15.53
PEDOT@ UiO-66	30.02	121.16	125.2x 10^{-6}	1.28	875.4	12.16

Only tetrahedral pores remained after the octahedral pores of UiO-66 were occupied by PEDOT chains, which has an impact on the diffusion of ions from electrolyte. Due to obstructions in the effective pathways caused by pre-filled pores, PEDOT@UiO-66 exhibits a higher Warburg impedance, which suggests slower diffusion. The CPE exponent (*a*) is less than 1 for all the electrodes which indicates the non-ideal capacitive behaviour of the materials. The impedance due to CPE (Y_o) is characterized by a frequency-dependent phase angle that deviates from the ideal -90° phase angle of a perfect capacitor. The EIS results are in accordance with the CV results where the PEDOT@UiO-66 electrode exhibited highest current response to the potential thereby offering lower obstacles in the electron transfer pathways between the electrode and $[Fe(CN)_6]^{3-/4}$.

6.3 Optimization of sensing parameters

6.3.1 Cyclic Voltammetry in presence of analytes HQ and CT

To investigate the response of ITO, UiO-66 and PEDOT@UiO-66 to analytes HQ and CT 0.1 μM of the analytes were added in 0.1 M Tris Buffer Saline (TBS) solution and CV was performed at a scan rate of 10 mV/s (Fig. 6.4 (a)). In the TBS solution ITO was unable to detect the two analytes separately and showed a broad oxidation peak with very low current response. On the other hand, UiO-66 also failed to differentiate the redox response of CT and HQ to the electrode. When the PEDOT@UiO-66 composite was used to modify the ITO electrode, the material responded to two analytes independently. Here from the voltammogram it is clear that there are two peaks at 0.083 V and 0.30 V which corresponded to HQ and CT oxidation peak while HQ and CT reduction peaks are located at 0.139 V and -0.016 V. The redox peak separation (ΔE) for HQ is found to be 0.0189 V while for CT it is 0.164 V. Also, the ratio of redox peak current (I_{pa}/I_{pc}) ~ 1 while interacting with HQ. Thus, the reaction taking place at the surface of PEDOT@UiO-66 with HQ can be considered as the reversible one while with CT the reaction is quasi reversible one according to the established theories. Another interesting result is that the peak current is also enhanced in case of PEDOT@UiO-66 after incorporation of PEDOT in UiO-66. The area covered under the cyclic voltammogram is a representation of the total charge stored during the faradic and non-faradic processes. In comparison to ITO and UiO-66, PEDOT@UiO-66 presents a larger area, indicating that more charges have been stored or that a larger concentration of charges participated in the charge transfer process. The response of pristine PEDOT fabricated on ITO glass was also checked for its affinity towards the analytes as shown in Fig. 6.4 (b). Even in a large potential window of -1.5 V to 1.5 V, distinguished peaks of HQ and CT are not resolved. This says that PEDOT individually cannot differentiate the isomers.

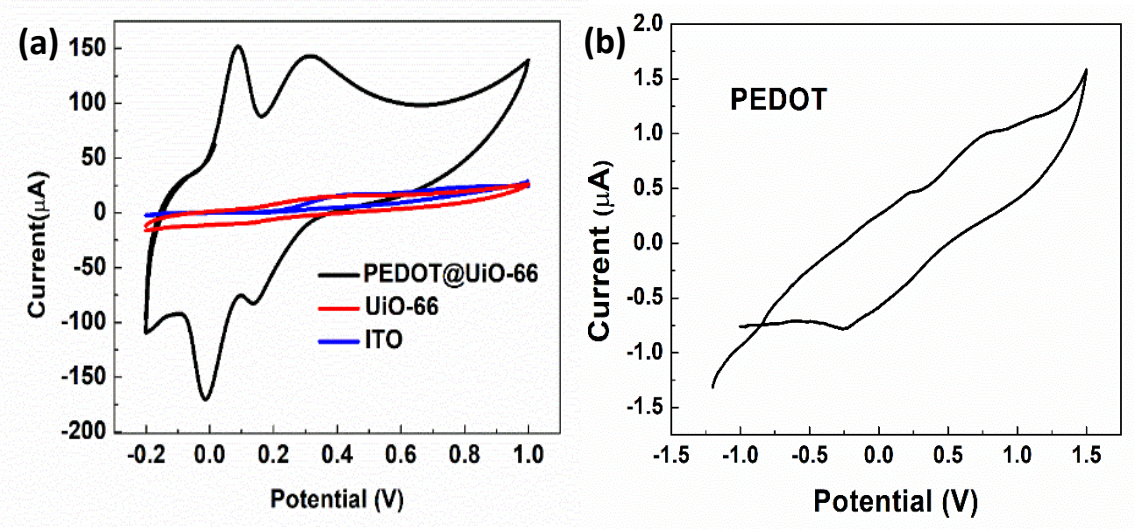

Fig. 6.4. CV response of (a) ITO, UiO-66 and PEDOT@UiO-66 and (b) PEDOT towards CT and HQ.

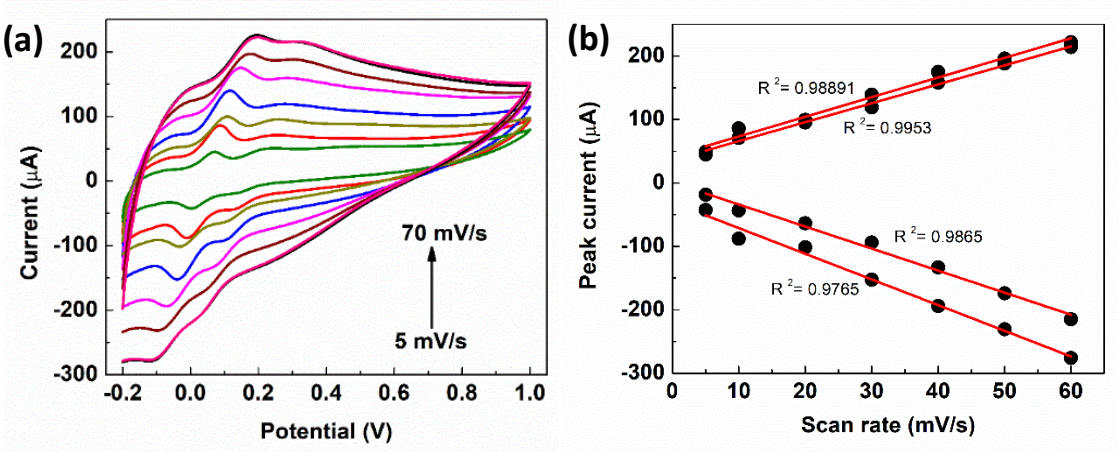

Fig. 6.5. (a) Scan rate varying CV of PEDOT@UiO-66 in the presence of CT and HQ, (b) Linear regression curve of scan rate and peak current.

While the scan rate was increased from 5 mV/s to 70 mV/s in the presence of both the analytes, a linear increase has been observed in the peak current up to 60 mV/s and further there is no increase in the peak current with increasing scan rate. The linearity between peak currents of HQ and CT and scan rate are shown in Fig. 6.5 (a) and (b) and are represented with linear regression relations as -

$$I_{paHQ} = 3.09 \times 10^{-6}\, \upsilon + 4.22 \times 10^{-5} \quad (6.6)$$

$$I_{pcHQ} = -4.04 \times 10^{-6}\, \upsilon - 3.06 \times 10^{-6} \quad (6.7)$$

$$I_{paCT} = 2.98 \times 10^{-6}\, \upsilon + 3.6 \times 10^{-5} \quad (6.8)$$

$$I_{pcCT} = -3.474 \times 10^{-6}\, \upsilon + 7.7 \times 10^{-7} \quad (6.9)$$

From these results one may conclude that the reaction that has taken place between CT and HQ are controlled by surface-controlled phenomenon where the rate of the electrochemical reaction is determined by the kinetics of the electron transfer taking place at the interface of electrode and electrolyte solution.

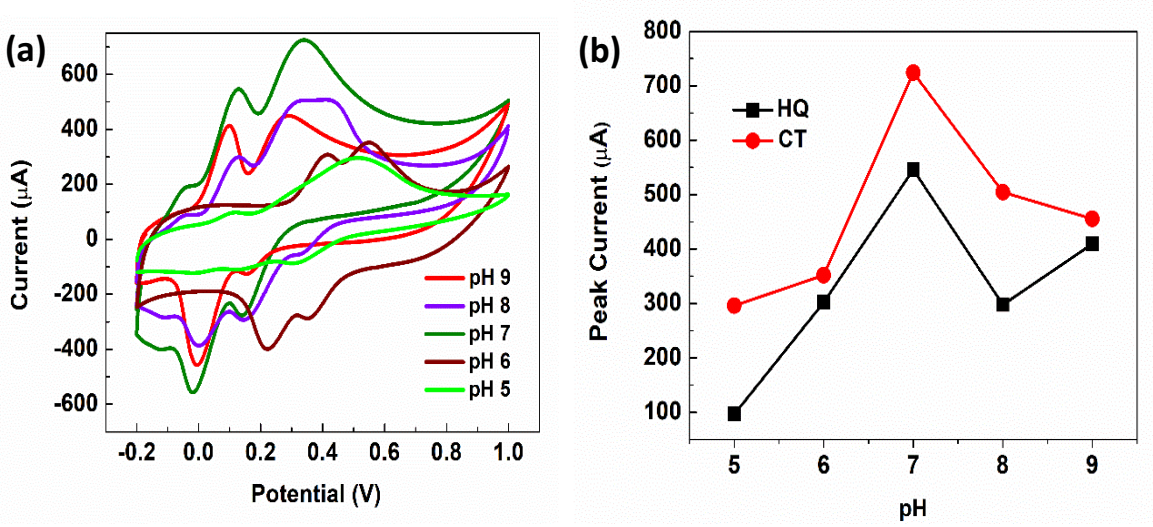

Fig. 6.6. (a) CV of PEDOT@UiO-66 with inclusion of CT and HQ at different pH and (b) pH vs. peak current.

6.3.2 Effect of pH on the redox reactions

In an electrochemical process pH of the electrolyte can influence the protonation/deprotonation of the species present in the electrolyte as the interaction of protons or hydroxide ions with the electrode can hinder the charge transfer event and overall reaction kinetics. Therefore, optimizing the pH of the supporting electrolyte is necessary during the electrochemical experiments. The pH of the electrolyte was varied from 5 to 9 and CV pattern was monitored for each value of pH (Fig. 6.6 (a), (b)). The peak current was seen to get increased from pH 5 to 7 and get it declined afterward. Also, the peak position was varied with changing pH. This indication is attributed to the influence of protons in the redox reactions. After a close observation on the results, pH 7 was opted as the optimal value for the rest of reactions.

6.4.Analysis of individual and simultaneous electrochemical sensing of Catechol (CT) and Hydroquinone (HQ) using PEDOT@UiO-66 working electrode

6.4.1 Sensing of HQ and CT individually

The concentration of HQ in TBS was varied from 1 µM to 300 µM in order to obtain the quantitative response of HQ towards PEDOT@UiO-66. The redox peak current increased linearly when the concentration was varied between 1 µM to 300 µM, as shown in Fig. 6.7 (a). The linearity relation of concentration and peak current density is given by equation 6.6. The LOD has been calculated using the slope of the linear plot (Fig. 6.7 (b)) and

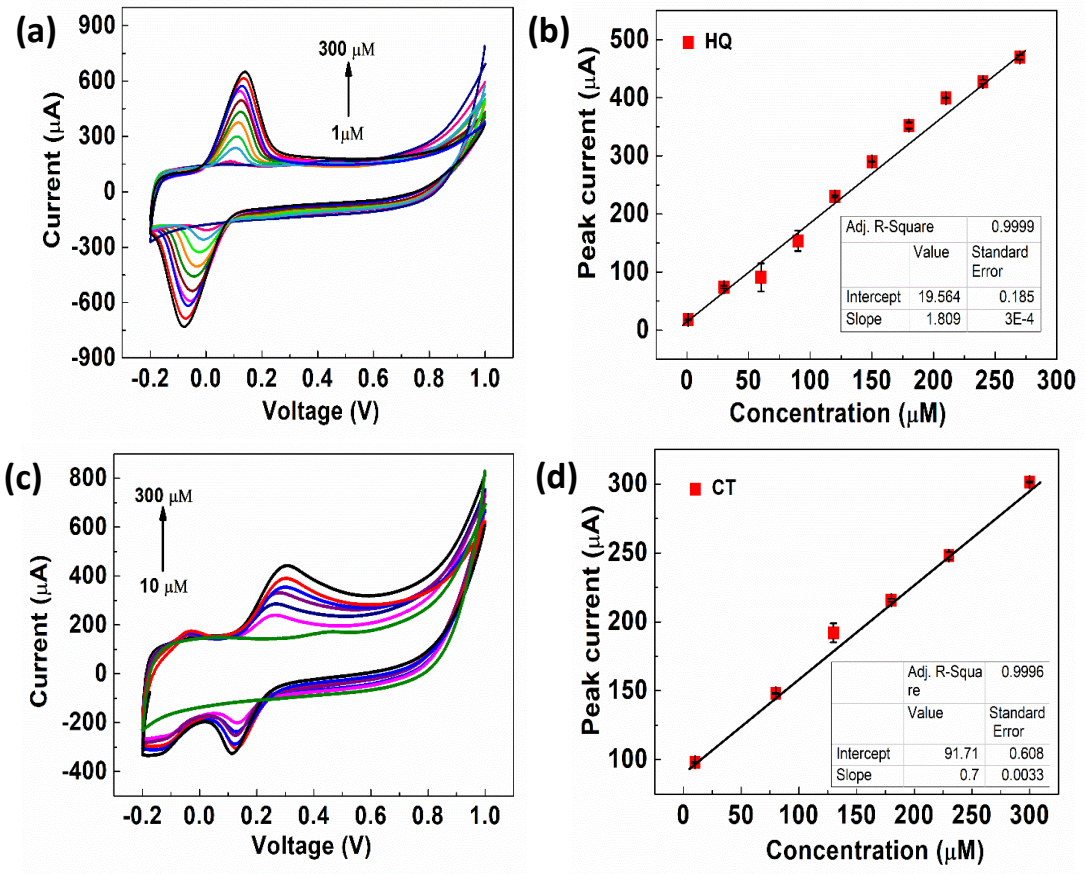

Fig. 6.7. (a) CV of PEDOT@UiO-66 sensing HQ with different concentration, (b) calibration plot of current density of anodic peak and HQ concentration, (c) CV of PEDOT@UiO-66 sensing CT with different concentration, (d) calibration plot of current density of anodic peak and CT concentration.

equation LOD= $3.3 \times S_y/m$, where S_y is the standard error and m is the slope . The value of LOD calculated by considering the anodic peak was is 0.338 μM and sensitivity was 1.809 μA $\mu M^{-1}cm^{-2}$.

$$I_{pa}\ (\mu A) = 1.809\ C\ (\mu M) - 19.564\ ,\ R^2 = 0.9999 \qquad (6.10)$$

In a similar manner, concentration of CT was varied from 10 μM to 300 μM and CV patterns have been acquired, shown in Fig. 6.7 (c). For the anodic reaction the peak current increases with concentration.The linearity was found in anodic reaction in the concentration range of 10 μM-300 μM given by the equation-

$$I_{pa}(\mu A) = 0.7\ C\ (\mu M) + 91.71\ ,\ R^2 = 0.9996 \qquad (6.11)$$

The detection limits and sensitivity were calculated using the slope and intercept of linear regression plot of concentration of CT vs. peak current and are found to be 2.84 μM and 0.7 μA $\mu M^{-1}cm^{-2}$.

The sensing of HQ and CT independently is carried out in two additional PEDOT@UiO-66 electrodes to confirm the reproducibility of the electrode. All the electrodes detected the HQ, with a standard deviation (SD) of ± 0.101 in the LOD values and ± 0.411 (μA $\mu M^{-1}cm^{-2}$) in the sensitivity values. In a similar manner, the other two PEDOT@UiO-66 sensors detected CT with an SD of 0.179 for the LOD and a sensitivity of ± 0.0954 μA μM-1cm-2. The LOD and sensitivity values obtained for all the three electrodes of PEDOT@UiO-66 are shown in Fig. 6.8 (a) and (b).

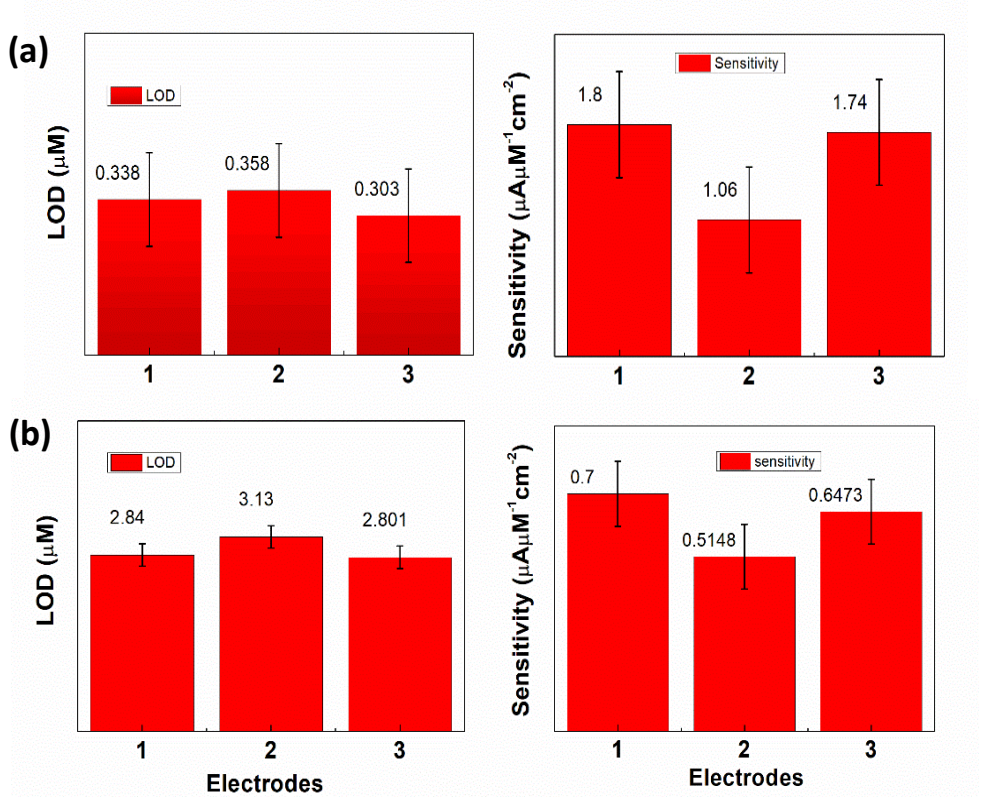

Fig. 6.8. LOD and sensitivity values of (a) HQ and (b) CT sensing individually by three different working electrodes of PEDOT@UiO-66 represented as histogram with standard deviation as error bars.

6.4.2 Simultaneous sensing of HQ and CT by PEDOT@UiO-66 MOF

For simultaneous sensing different concentration of CT and HQ were added to the supporting electrolyte at same time . The PEDOT@UiO-66 was able to obtain resolved peaks of HQ and CT at two defferent potentials (0.141V and 0.36 V). When the concentration of HQ and CT were varied from 10 µM to 320 µM the peak current of HQ and CT got increased (Fig. 6.9 (a)). The corresponding linear regression equations for anodic peaks are given by eqn. 6.8 and 6.9.

$$I_{paHQ}(\mu A) = 0.416\, C(\mu M) + 72.16 \text{ , } R^2 = 0.9999 \qquad (6.12)$$

$$I_{paCT}(\mu A) = 0.389\, C\ (\mu M) + 66.75 \text{ , } R^2 = 0.9992 \qquad (6.13)$$

The linear-range for HQ and CT is 10-320 µM . The slope of linear plots have been used to calculate the value of LOD and sensitivities. Here, limit of detection(LOD) for HQ and

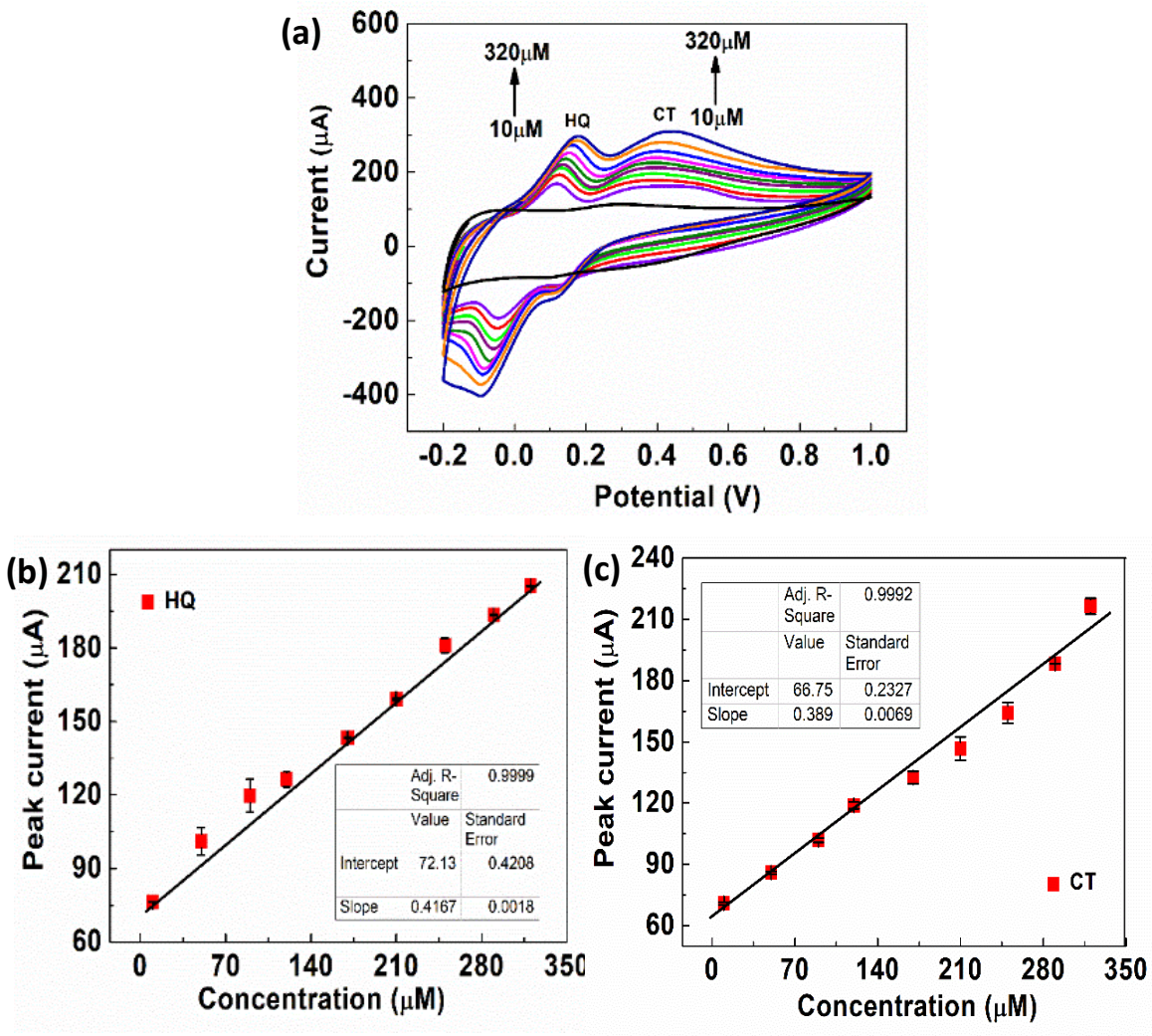

Fig. 6.9. (a) CV of PEDOT@UiO-66 sensing HQ and CT simultaneously with varying concentration from 10 μM to 320 μM, (b) and (c) calibration plots of peak current vs. concentration of HQ and CT respectively.

CT are found to 3.3 μM and 1.98 μM, respectively. When the analytes were used simultaneously we found different value for sensitivity in comparision to individual sensing i.e, 0.416 μA $\mu M^{-1}cm^{-2}$ for HQ and 0.3890 μA $\mu M^{-1}cm^{-2}$ for CT (Fig. 6.9 (b) and (c)).

6.4.3 Selective detection of HQ and CT from their mixtures

By varying the concentration of one component while maintaining the concentration of the other isomer constant, the specificity of the PEDOT@UiO-66 MOF towards determing HQ, CT in their mixed components was considered. The response of CV redox peaks of

PEDOT@UiO-66 when the concentration of HQ was varied from 10 μM to 240 μM in presence of 250 μM CT can be found from Fig. 6.10 (a) . The peak current of HQ increased gradually with concentration while peak current of CT remains constant as expected. The linear regression relation is obtained from the anodic peak shown in Fig. 6.10 (b) and the relevant equation is given by-

$$I_{pa}(\mu A) = 0.65\ C(\mu M) + 23.61 \qquad (6.14)$$

The LOD of HQ in the mixture of CT is calculated using the slope and signal to noise ratio 3.3 to be 3.21 μM. Simillarly CT was also detected in a mixture of 30 μM HQ when the concentration was varied from 10 μM- 150 μM. The redox peak current of CT gets increased linearly with increasing concentration shown in Fig. 6.10 (c). The linearity in the relationship of concentration and peak current density is shown in Fig.6.10 (d) and given by the equation-

$$I_{pa}(\mu A) = 0.635\ C(\mu M) + 15.41 \qquad (6.15)$$

The LOD was found to be 4.16 μM for CT in a mixture of its para isomer. These findings demonstrate PEDOT's selectivity and sensitivity for particular analytes in presence of other isomers.

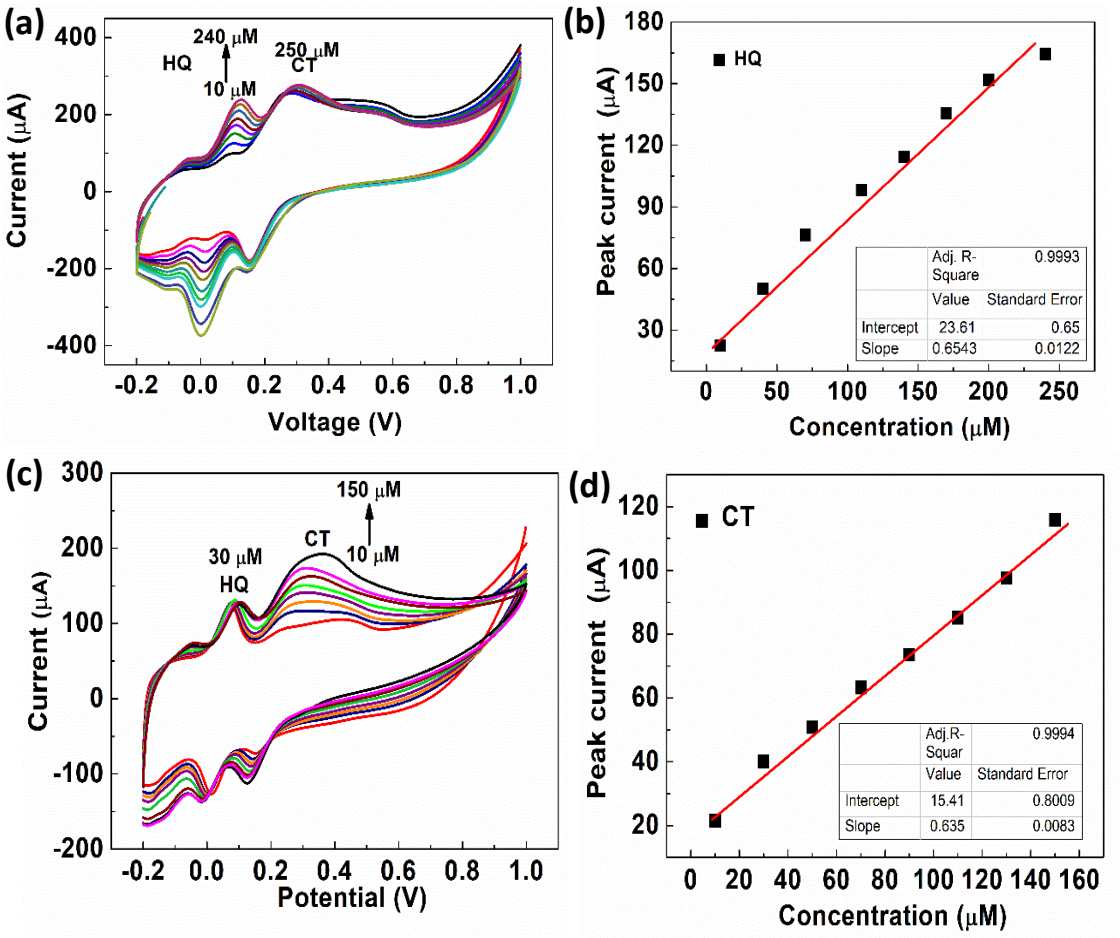

Fig. 6.10. (a) CV of PEDOT@UiO-66 detecting HQ at different concentration with keeping concentration of CT constant (b) calibration plot of peak current vs. concentration of HQ, (c) CV of PEDOT@UiO-66 detecting CT at different concentration with keeping concentration of HQ constant (d) calibration plot of peak current vs. concentration of CT.

6.4.4 Selectivity, Stability, repeatability and reproducibility

The CV were taken in 50 µM CT and 100 HQ in the presence of various interfering analytes such as Hg^{2+}, Cd^{2+}, Ni^{2+}, Zn^{2+}, Pb^{2+}, Cu^{2+}, K^{+} to confirm the selectivity of PEDOT@UiO-66 towards the required analytes. The interfering analytes had a concentration of 0.01 mM. When other analytes were added to the electrolyte, no further peak was noticed, and the current response of CT and HQ remained constant with RSD of ±3% and ±2.8% (Fig. 6.11 (a) and (b)). Consequently, the results demonstrate high selectivity of PEDOT@UiO-66 towards CT and HQ.

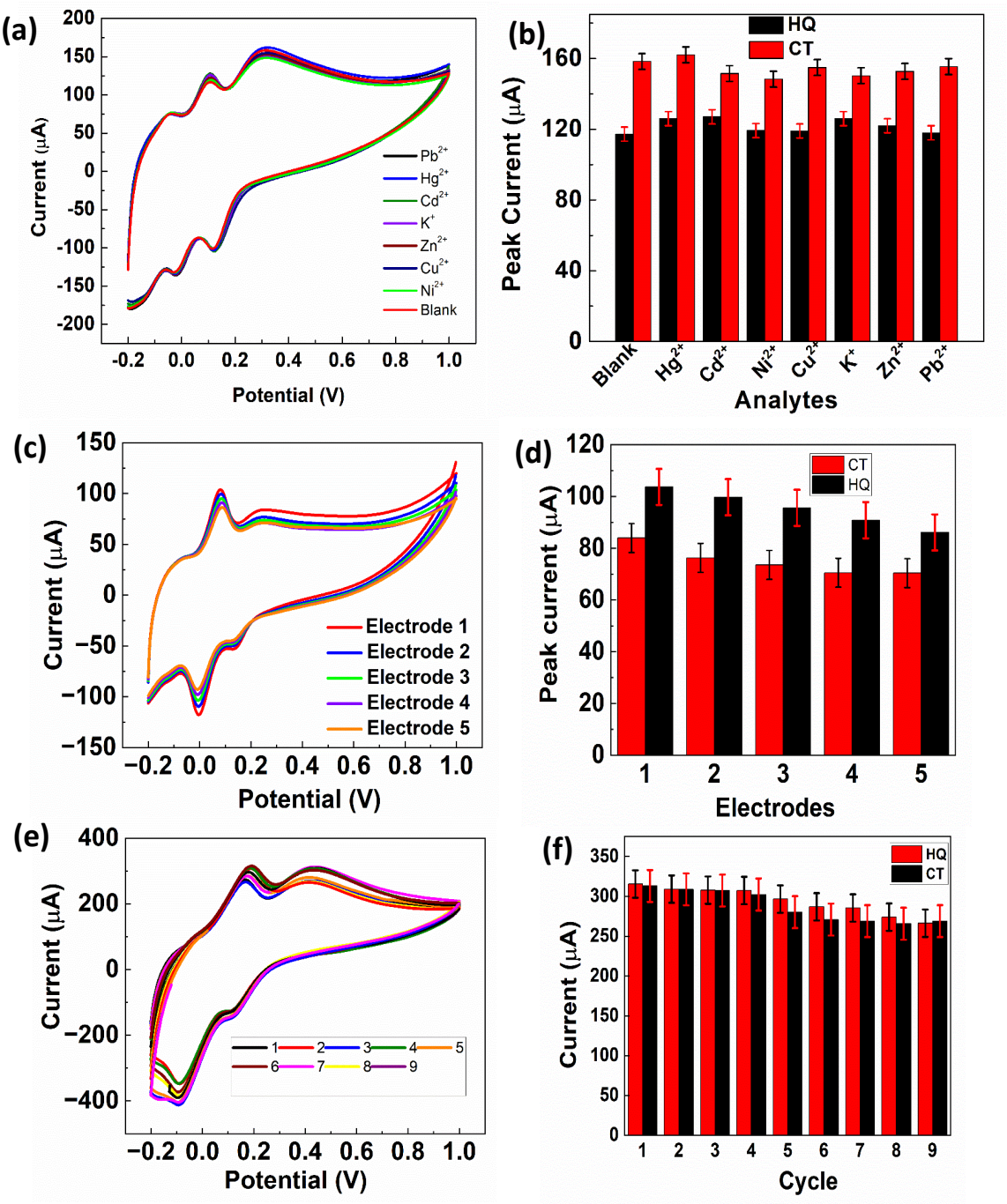

Fig. 6.11. (a) CV of PEDOT@UiO-66 in response to HQ and CT in presence of different interfering analytes, (b) histogram of peak Current of CT and HQ in presence of other analytes (c) CV of 5 electrodes of PEDOT@UiO-66 in response to CT and HQ (d) histogram representing the deviation in peak current of 5 electrodes of same kind (e) CV of PEDOT@UiO-66 in response to 0.5 μM CT and HQ for 9 cycles and (f) histogram representing the deviation in peak current of 9 CV cycles.

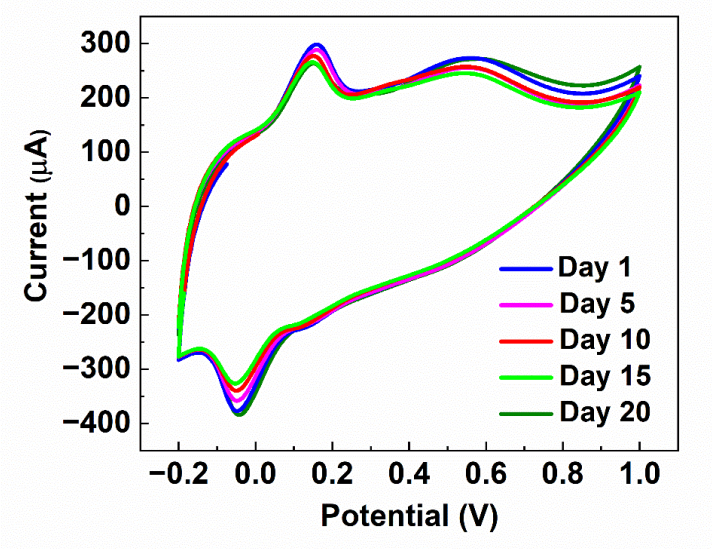

Fig. 6.12. CV of PEDOT@UiO-66 in response to 0.5 μM CT and HQ by storing up to 20 days.

Reproducibility of the results were observed by taking CV of 5 electrodes of same kind (PEDOT@UiO-66) in presence of 50M HQ and 20 μM CT (Fig. 6.12 (c)). All five electrodes offered nearly similar voltammograms with the obvious redox peaks of HQ and CT. The relative standard deviation of the 5 data were found to be ±7.4% for HQ and ±7.3% for CT. The repeatability of results was measured by taking 9 consecutive CV cycles with 50 μM CT and HQ in TBS. The cycles remain stable with an RSD of ±5.8 % for HQ and ± 6% for CT.

The stability of the prepared electrode with PEDOT@UiO-66 was determined by taking the CV response of the electrode after every 5 days for 20 days by storing it in room temperature shown in Fig. 6.12. The current response of PEDOT@UiO-66 remained 87.9%-96.6% and 89.3%-98.9% of their response on the first day, while considering their interaction with HQ and CT after 20 days. Consequently, a good stability of the prepared electrode has been ensured in terms of sensing capability.

6.4.5 Real Sample analysis

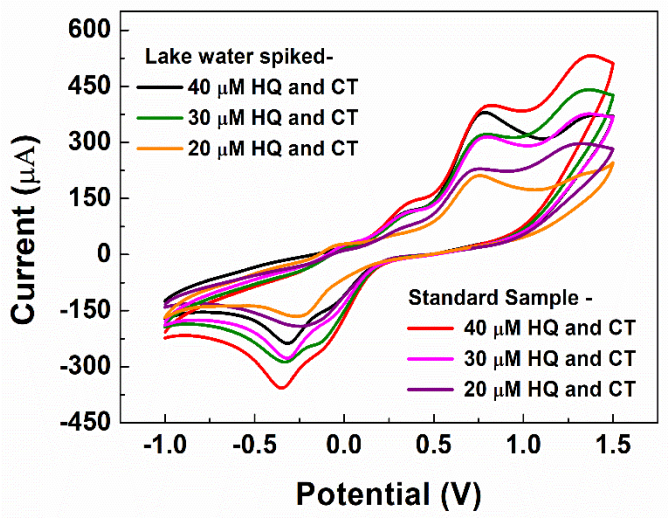

Fig. 6.13. Detection of CT and HQ by PEDOT@UiO-66 in real lake water sample.

To evaluate the applicability of PEDOT@UiO-66 for simultaneous detection of HQ and CT in real samples tape water and lake water were used. Standard addition method has been used for the analysis. At optimised condition of CV of tape water were measured which shows no particular peak at a potential window of -0.4V to 1.2 V. Therefore, different amount of HQ and CT were added to the tape water and analysed with PEDOT. The recoveries at different concentrations were tabulated in Table 6.3 which falls in the range of 90-93% for HQ and 91-96% for CT. The RSD were calculated to be 0.36 and 0.68 for HQ and CT respectively. This clearly indicates the effective simultaneous detection of CT and HQ by the electrode PEDOT@UiO-66 in real water samples.

Table 6.3 Results of HQ and CT detection in local lake water sample by PEDOT@UiO-66 MOF systems

Sample	**Detected (μmol L^{-1})**		**Added (μmol L^{-1})**		**Concentration recovered (μmol L^{-1})**		**Recovery (%)**		**RSD (%)**	
	HQ	CT	HQ	CT	HQ	CT	HQ	CT	HQ	CT
Lake water	0.0	0.0	20	20	17.9 ± 0.7	18.9 ± 0.77	85.8	92.1	7.8	3.9
	0.0	0.0	30	30	29.5 ± 1.2	29.3 ± 1.01	98.6	97.8	1.6	1.1
	0.0	0.0	40	40	36.4 ± 2.8	35.1 ± 2.2	91.1	95.9	6.6	9.2

6.5 Conclusion

The benefit of incorporation of PEDOT into the framework of UiO-66 in carrier transport phenomenon was established chapter 4. Here, this chapter was focused on the application of PEDOT@UiO-66 in the electrochemical sensing of dihydroxy benzene isomers. PEDOT@UiO-66 was fabricated on the ITO glass in order to form a working electrode for the sensing set-up through slurry coating methods. After incorporation of PEDOT into the pores of UiO-66 the electrochemical properties got enhanced as expected. The multiple benefits like porosity, conductivity, large surface area guarantee the easy adsorption as well as exchange of electrons with the target analytes. As a result, the electrode could easily distinguish the two isomers with a profound sensitivity over a wide range of concentration of analytes. Moreover, the desired property of an electrochemical sensor is its specificity for target analyte which was well established by PEDOT@UiO-66 while the analytes were interfered with unwanted analytes. The results were seen to be reproducible and repeatable while offering a long-term stability. Due to the easy processing of PEDOT@UiO-66, friendly fabrication method and its affinity for HQ and CC detection, these composites for electrochemical sensors may spark increased research interest.

References

[1] Varjani, S. J. & Upasani, V. N. A new look on factors affecting microbial degradation of petroleum hydrocarbon pollutants. *Int Biodeterior Biodegradation*. **120**: 71–83, 2017.

[2] Zou, X. *et al.* Recent advances of environmental pollutants detection via paper-based sensing strategy. *Luminescence*. **36**: 1818–1836, 2021.

[3] Abugazleh, M. K., Ali, H. M., Chester, J. A., Al-Fa'ouri, A. M. & Bouldin, J. L. Aquatic toxicity of hydroquinone and catechol following metal oxide treatment to Ceriodaphnia dubia and Pimephales promelas. *Ecotoxicology*. **32**: 656–665, 2023.

[4] Lee, B. L., Ong, H. Y., Shi, C. Y. & Ong, C. N. Simultaneous determination of hydroquinone, catechol and phenol in urine using high-performance liquid chromatography with fluorimetric detection. *J Chromatogr B Biomed Sci Appl*. **619**: 259–266, 1993.

[5] Nsanzamahoro, S. *et al.* Highly selective and sensitive detection of catechol by one step synthesized highly fluorescent and water-soluble silicon nanoparticles. *Sens Actuators B Chem*. **281**: 849–856, 2019.

[6] Zhao, L., Lv, B., Yuan, H., Zhou, Z. & Xiao, D. A Sensitive Chemiluminescence Method for Determination of Hydroquinone and Catechol. *Sensors*. **7**: 578–588, 2007.

[7] Meskher, H. & Achi, F. Electrochemical Sensing Systems for the Analysis of Catechol and Hydroquinone in the Aquatic Environments: A Critical Review. *Crit Rev Anal Chem*. **25**: 1–14, 2022.

[8] Privett, B. J., Shin, J. H. & Schoenfisch, M. H. Electrochemical Sensors. *Anal Chem*. **82**: 4723–4741, 2010.

[9] Huang, H. *et al.* Electrochemical sensor based on Ce-MOF/carbon nanotube composite for the simultaneous discrimination of hydroquinone and catechol. *J Hazard Mater*. **416**: 125895, 2021.

[10] Kitao, T., Zhang, Y., Kitagawa, S., Wang, B. & Uemura, T. Hybridization of MOFs and polymers. *Chem Soc Rev*. **46**: 3108–3133, 2017.

[11] Freund, R. *et al.* The Current Status of MOF and COF Applications. *Angewandte Chemie International Edition*. **60**: 23975–24001, 2021.

[12] Li, J. H., Wang, Y. Sen, Chen, Y. C. & Kung, C. W. Metal-organic frameworks toward electrocatalytic applications. *Applied Sciences (Switzerland)*. **9**: 2427, 2019.

[13] Wang, T. *et al.* Functional conductive nanomaterials via polymerisation in nano-channels: PEDOT in a MOF. *Mater Horiz*. **4**: 64–71, 2017.

[14] Chen, Q. *et al.* Determination of catechol and hydroquinone with high sensitivity using MOF-graphene composites modified electrode. *Journal of Electroanalytical Chemistry*. **789**: 114–122, 2017.

[15] Xin, Y. *et al.* Electrochemical detection of hydroquinone and catechol with covalent organic framework modified carbon paste electrode. *Journal of Electroanalytical Chemistry*. **877**: 114530, 2020.

[16] Abdel-Aziz, A. M., Hassan, H. H., Hassan, A. A. & Badr, I. H. A. A Sensitive and Green Method for Determination of Catechol Using Multi-Walled Carbon Nanotubes/Poly(1,5-diaminonaphthalene) Composite Film Modified Glassy Carbon Electrode. *J Electrochem Soc*. **166**: B1441–B1451, 2019.

[17] Manjunatha, J. G. A surfactant enhanced graphene paste electrode as an effective electrochemical sensor for the sensitive and simultaneous determination of catechol and resorcinol. *Chemical Data Collections*. **25**: 100331, 2020.

[18] Andrienko, D. *Cyclic Voltammetry* (2008).

[19] Paixão, T. R. L. C. Measuring Electrochemical Surface Area of Nanomaterials versus the Randles−Ševčík Equation. *ChemElectroChem*. **7**: 3414–3415, 2020.

[20] Brown, A. P. & Anson, F. C. Cyclic and differential pulse voltammetric behavior of reactants confined to the electrode surface. *Anal Chem*. **49**: 1589–1595, 1977.